THE JOURNAL OF PHYSICAL CHEMISTRY Letters

Letter

Cite This: J. Phys. Chem. Lett. 2019, 10, 4632−4638

pubs.acs.org/JPCL

Tuning Optical Properties of Conjugated Molecules by Lewis Acids: Insights from Electronic Structure Modeling

Hung Phan,[†,‡] Thomas J. Kelly,[§] Andriy Zhugayevych,[∥] Guillermo C. Bazan,[‡] Thuc-Quyen Nguyen,[‡] Emily A. Jarvis,*[,§] and Sergei Tretiak*[,‡,∥,⊥]

[†]Fulbright University Vietnam, Ho Chi Minh City, Vietnam

[‡]Center for Polymers and Organic Solids (CPOS), University of California Santa Barbara, Santa Barbara, California 93106, United States

[§]Department of Chemistry & Biochemistry, Loyola Marymount University, Los Angeles, California 90045, United States

[∥]Skolkovo Institute of Science and Technology, Moscow 143026, Russia

[⊥]Theoretical Division and Center for Integrated Nanotechnologies, Los Alamos National Laboratory, Los Alamos, New Mexico 87545, United States

Supporting Information

ABSTRACT: Understanding and controlling the optoelectronic properties of organic semiconductors at the molecular level remains a challenge due to the complexity of chemical structures and intermolecular interactions. A common strategy to address this challenge is to utilize both experimental and computational approaches. In this contribution, we show that density functional theory (DFT) calculation is a useful tool to provide insights into the bonding, electron population distribution, and optical transitions of adducts between conjugated molecules and Lewis acids (CM−LA). Adduct formation leads to relevant modifications of key properties, including a red shift in optical transitions and an increase in charge carrier density and charge mobility, compared to the parent conjugated molecules. We show that electron density transfer from the CM to the LA, which was hypothesized to cause the experimental red shift in absorption spectra upon LA binding, can be quantified and interpreted by population analysis. Experimental red shifts in optical transitions for all molecular families can also be predicted by time-dependent DFT calculations with different density functionals. These detailed insights help to optimize a priori design guidelines for future applications.

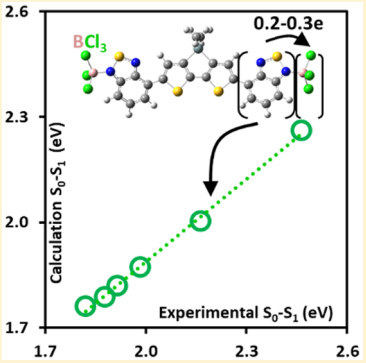

Optoelectronic processes in organic semiconductors have intrigued scientists for several decades. Understanding certain phenomena at the molecular level remains a challenge due to the complexity of chemical structures and intermolecular interactions. Continued improvement and refinement of organic semiconductors relies on an immense number of chemical structures.[1−11] New families of organic and hybrid semiconductors are being continuously designed and studied. One encouraging path for methodically tuning key properties involves the adducts of conjugated molecules and Lewis acids (CM−LA).[12−22] These adducts are formed by the partial electron density transfer from a semiconducting conjugated molecule or polymer, usually containing a Lewis base (LB) site to an external Lewis acid (LA). Boron-based LAs such as BF_3, BCl_3 and $B(C_6F_5)_3$ (with the three fluorinated benzene rings abbreviated as CF) have been widely utilized. The resulting adducts have been experimentally demonstrated to have interesting optoelectronic properties, including a red shift in optical transitions,[12−14,19,21,22] and an increase in charge carrier density compared to the parent conjugated molecules.[15,16,18] The underlying principles of these changes require further investigation from both experimental and computational perspectives. In this Letter, we provide insights into the interaction between CM and LA, electron population distribution, and optical transitions of CM−LA adducts using density functional theory (DFT) calculations. Understanding and controlling these trends via structural modifications may facilitate applications of these adducts in organic electronics and benefit the development of novel compounds incorporating coordination bonds such as B ← N.[23,24]

Since the first report of the CM−LA adduct in 2009,[12] there have been several investigations of CM−LA adducts, mainly employing experimental techniques.[12−16,18,20,25−29] Most of the molecules in these studies have an alternating donor−acceptor (D−A) motif, in which the acceptor unit contains atoms with a nonbonding pair of electrons capable of coordinating with LAs. In this study, we chose three D−A molecules, denoted J09G1, J11G3, and J11G8, as model compounds (Supporting Information, section S1). Their chemical structures, presented in Figure 1a, contain either

Received: June 1, 2019
Accepted: July 10, 2019
Published: July 10, 2019

DOI: 10.1021/acs.jpclett.9b01572
J. Phys. Chem. Lett. 2019, 10, 4632−4638

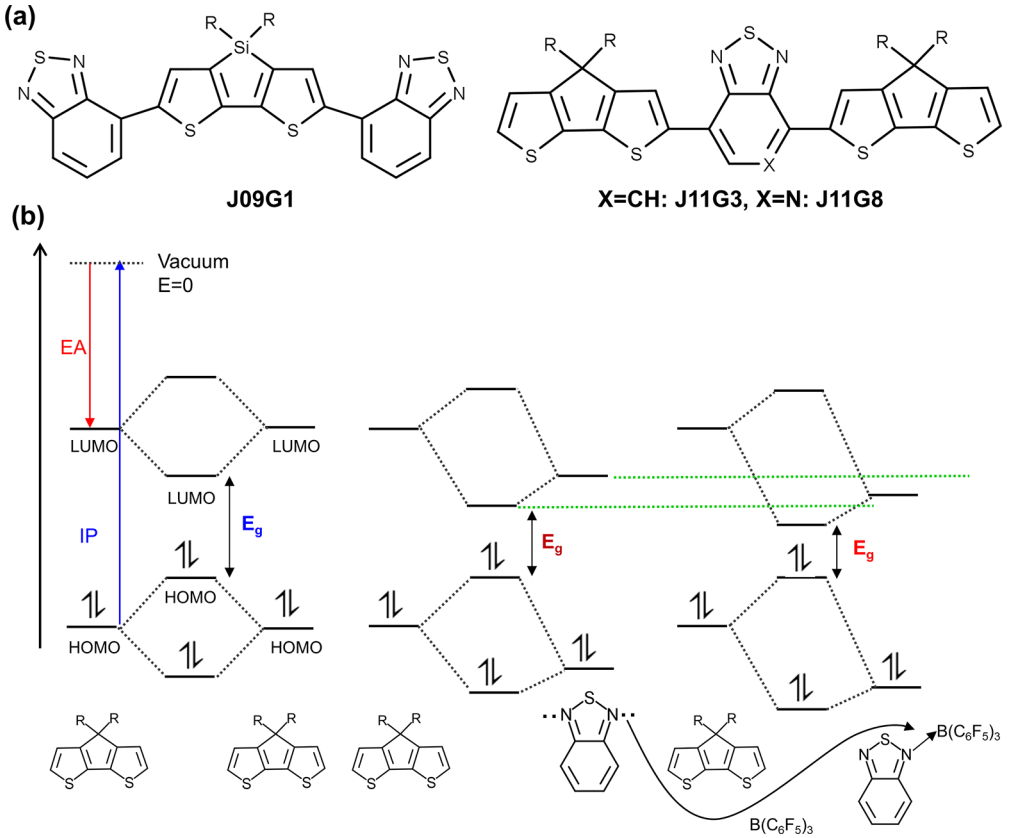

Figure 1. (a) Three model molecules used in this study, J09G1, J11G3, and J11G8, and (b) schematic representation of the hypothesis of optical bandgap reduction from the original interactions of what would be D−D regions of the monomer, transitioning to the D−A hybridization with energy of the acceptor lowered in both the occupied and virtual states, and finally the D−A bound to a LA where energy lowering of the acceptor states for hybridization is further magnified.

benzo-2,1,3-thiadiazole (BT) or pyridyl-2,1,3-thiadiazole (PT) as the electron-acceptor unit.

Despite studies investigating the application of CM−LA adducts, few attempts have been made to explore and quantify physical processes underlying observed trends in optoelectronic properties of those adducts. Some of the first studies hypothesized that electron donation from the electron-poor fragment of the molecules to LAs is the fundamental cause. When this happens, the acceptor strength increases, hence reducing the bandgap of the molecule, as reflected in the consequential red-shifted optical transitions.[12−14] This explanation seems particularly relevant to D−A molecules, where bandgap reduction results from hybridization of the donor and acceptor moieties, as shown in Figure 1b. For example, in adducts of molecules containing either BT or PT as the electron-acceptor unit and BCF, the lone-pair orbital of nitrogen in their structure may donate an electron to boron's empty orbital in BCF. In this scenario, BCF draws electronic density from BT or PT, thus enhancing its acceptor strength.

Although this electron transfer in LA−LB bonds is intuitively understood in organic chemistry, it is challenging to confirm this process experimentally, especially for an adduct with bulky conjugated molecules. For small crystalline LA−LB adducts, high-resolution X-ray diffraction at low to very low temperatures coupled with multipole refinement and population analysis can be used only to roughly estimate the charge transfer from LB to LA.[30] It has been suggested that quantitative interpretation of experimental data even for these small systems should be coupled with theoretical calculations.[30] Accordingly, in this contribution, we first aim to characterize the charge transfer from the LB moiety to the LA by DFT calculations and subsequently analyze the optical transitions of the adducts.

In the realm of electronic structure theory, prediction of structural motifs,[31,32] conformations,[33,34] and electronic features (particularly related to electronic transfer processes)[35−40] are subject to the choice of proper level of theory. For DFT, the presence of a fractional contribution of the orbital exchange is perhaps the most important parameter. Consequently, prior to characterizing charge transfer and optical properties, we tested several commonly used functionals and basis sets to optimize the geometry of the parent molecules and adducts. To model the electrostatic effects of a solvent in all calculations, we use the conductor-like polarizable continuum model (CPCM).[41−43,35] All results presented in this Letter are calculated with the 6-311G(d,p) basis set.

Structural properties of the adducts including the length of coordination bonds between LA and LB, binding energy, and dihedral angle changes are summarized in Figure S1 and Table S1, Supporting Information. The DFT-calculated N−B bond lengths (1.58−1.68 Å) and binding energies (~100 kJ/mol) are consistent with previous experimental and theoretical values for a wide range of small LB−LA complexes (such as NH_3:BF_3) reported in the literature.[44,45] We subsequently used time-dependent DFT (TD-DFT) to calculate the S_0−S_1 transition of the adducts. Of the popular functionals we have tried, CAM-B3LYP-D3[46,47] (thoroughly tested in our previous works)[32,35] and APFD[48] (with incorporated dispersion

DOI: 10.1021/acs.jpclett.9b01572
J. Phys. Chem. Lett. 2019, 10, 4632−4638

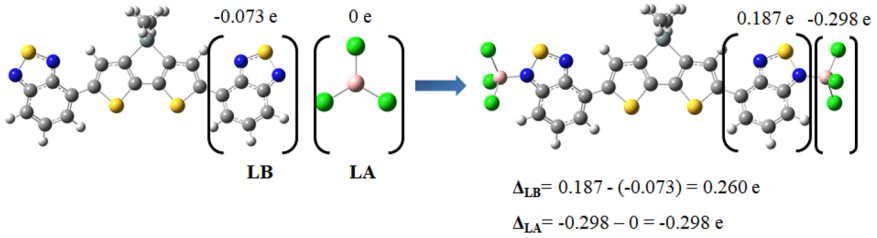

Figure 2. Illustration of charge transfer evaluated via DFT calculations and NBO analysis. Here, the CM−LA adduct (J09G1−2BCl_3) is calculated using APFD. The results of analogous calculations conducted across the adduct series are summarized in Table 1.

Table 1. Charge Transfer Quantification of CM−LA Adducts Including J09G1, J11G3, and J11G8[a]

	NBO - vacuum				NBO - dichlorobenzene			
molecules and adducts	Σ_{LB}[b]	Δ_{LB}[c]	Δ_{LA}[d]	Δ_{LB} + Δ_{LA}	Σ_{LB}[b]	Δ_{LB}[c]	Δ_{LA}[d]	Δ_{LB} + Δ_{LA}
J09G1	−0.073				−0.063			
J09G1−$AlMe_3$	0.036	0.109	−0.129	−0.020	0.057	0.120	−0.146	−0.027
J09G1−$AlEtCl_2$	0.026	0.099	−0.133	−0.034	0.042	0.105	−0.159	−0.054
J09G1−AlCF	0.060	0.133	−0.171	−0.039	0.077	0.141	−0.186	−0.045
J09G1−BCF	0.261	0.334	−0.373	−0.039	0.284	0.347	−0.393	−0.046
J09G1−BCl_3	0.187	0.260	−0.298	−0.038	0.223	0.286	−0.343	−0.057
J09G1−BBr_3	0.157	0.230	−0.268	−0.038	0.196	0.259	−0.317	−0.058
J11G3	−0.162				−0.155			
J11G3−BCF	0.172	0.335	−0.372	−0.038	0.197	0.351	−0.389	−0.038
J11G8	−0.213				−0.213			
J11G8−BCF	0.031	0.244	−0.366	−0.122	0.072	0.286	−0.381	−0.096

[a]The values were calculated with APFD. [b]Σ_{LB}: total net charge of all atoms in the LB fragment of the molecule. [c]Δ_{LB}: change in total net charge of the LB fragment before and after binding to LA. [d]Δ_{LA}: change in total net charge of the LA fragment before and after binding to LA.

correction) models show stronger correlation between calculated and experimental red shifts in the S_0−S_1 transition. Therefore, we utilized these two methods for calculations and analysis of other properties in all of the molecules.

Population analysis provides a convenient means to analyze molecular wave functions and assign net charges to each atom in a molecule. Thus, calculated charges before and after LA binding can reveal charge transfer from the LB moiety of the parent molecule to the LA. Both natural atomic (NBO analysis)[49,50] and charge model 5 (CM5)[51,52] charges were used in this study and proved insensitive to basis sets among those investigated. We analyzed the change in the sum of net charges of all atoms in the LA and LB units before and after binding, as illustrated in Figure 2. For example, in the calculation of the J09G1−2BCl_3 adduct with the APFD model, where the LA is BCl_3 and the LB is the BT moiety, BCl_3 is initially a neutral molecule with a total net charge of zero. After binding, the total net charge of BCl_3 in the adduct becomes −0.298 e, indicating a partial electron transfer (Figure 2). On the other hand, the BT moiety of J09G1 has a total net charge (Σ_{LB}) of −0.073 e before and 0.187 e after binding to BCl_3, respectively, corresponding to an effective donation of electronic density to BCl_3.

We performed population analysis of all adducts after optimizing their ground-state geometry within both APFD (Tables 1 and S2) and CAM-B3LYP (Table S3), including dielectric medium effects. The results (Tables 1 and S2 and S3) uniformly reveal a significant shift in electron density from the LB to LA in the adducts. We first analyze the charge transfer for the J09G1 series. With NBO, we observe that the charge transfer significantly increases from aluminum- (∼0.1−0.15 e) to boron- (∼0.27−0.38 e) based LAs, which is reasonable given that boron-based LAs are stronger acids. For small complexes such as NH_3:BH_3 and NH_3:BF_3, NBO calculations reveal similar ∼0.35 e partial charge transfer,[30] which is larger than experimental estimates.[30] The specific values are subject to the particular charge partitioning scheme used in simulations (e.g., NBO, Hirschfield, or CM5), as well as uncertainties present in the experimental measurements. Furthermore, we find that the dielectric medium presence (i.e., vacuum vs dichlorobenzene) only weakly increases the amount of charge transfer.

The difference between the charge that LAs gain (Δ_{LA}) and the charge that LB fragments donate (Δ_{LB}) upon binding is characterized by the sum of the two quantities (Δ_{LB} + Δ_{LA}). In all cases, the sums of these net charges before and after LA binding are negative, meaning that the electron density gained by LAs is greater than that donated exclusively by the LB moiety that immediately binds to the LA. This indicates that the LA + LB complex also withdraws electrons from other adjacent fragments of the molecule, namely, the donor region. In terms of magnitude, the sum (Δ_{LB} + Δ_{LA}) is ∼5−10 times smaller than the total charge transfer to the LA (Δ_{LA}), indicating that only a minor amount of charge is taken from other fragments of the molecule. Interestingly, the charge gained by a BCF (Δ_{LA}) is very similar among all systems considered, J09−BCF, J11G3−BCF, and J11G8−BCF. The charge donated from LB (Δ_{LB}) is also similar across the series, except for J11G8−BCF when BCF binds to pyridyl nitrogen. In this J11G8−BCF case, the sum of the Δ_{LA} and Δ_{LB} is larger (∼0.10−0.18 e), implying that other portions of the molecules contribute more charge to BCF in this adduct. This might be due to the high electron-withdrawing ability of pyridyl nitrogen in the PT unit. The trends observed for charge transfer obtained with APFD calculations are consistent with the results obtained using the CAM-B3LYP functional. This lends

DOI: 10.1021/acs.jpclett.9b01572
J. Phys. Chem. Lett. 2019, 10, 4632−4638

confidence to the applicability of DFT for charge transfer analysis in CM−LA adducts, with proper choice of functionals and population analysis methods.

Our population analysis provides quantitative support of the hypothesis in Figure 1b. Electron withdrawing of LAs upon binding increases the acceptor strength, which results in reduction of the bandgap and consequently the red shift in absorption. Qualitatively, this effect can be observed visually in the progression of the frontier molecular orbitals (highest occupied molecular orbital, HOMO, and lowest unoccupied molecular orbital, LUMO) for the parent molecule relative to those with LA additions. For example, Figure S2 displays the LUMO evolution for J09G1, J09G1−AlCF, and J09G1−BCF sequence. These images clearly illustrate that LA binding increases orbital localization to the acceptor region of the molecule compared to the original unbound molecule, where the orbital is spread over both the donor and acceptor regions. Nevertheless, such orbital visualization captures only qualitative features and trends in electronic states.[53]

To provide further quantitative support of the hypothesis in Figure 1b, we conducted a systematic analysis of the optical transition energies of the adducts. Specifically, using TD-DFT we computed the transition energy for the first excited state (i.e., S_0−S_1 transition) in all molecules and correlated those to experimental data (peak wavelength converted to energy; Figure 3 and Table S4).[12,13] First, we analyzed J09G1 adducts

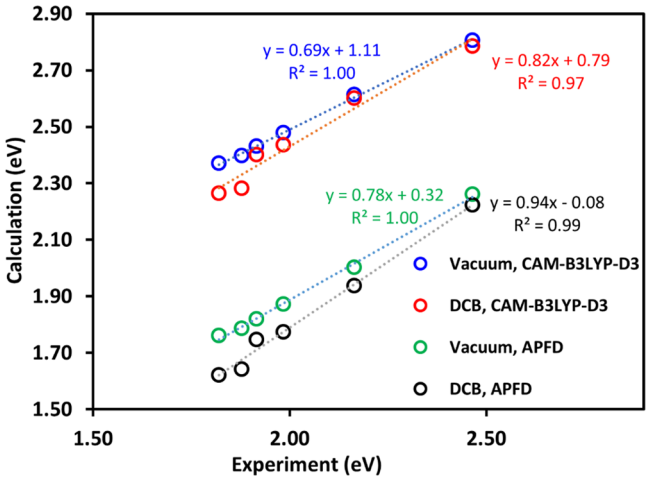

Figure 3. Correlation between calculated and experimental S_0−S_1 transition energies of the J09G1 series (see Table S4). Experimental S_0−S_1 transition energies are peak wavelengths converted to energy of UV−vis absorption data in *o*-dichlorobenzene (DCB) solvent. Calculated S_0−S_1 transition energies were carried out both in vacuum and in DCB medium.

when J09G1 binds to a series of LAs with different strengths, ranging from trimethylaluminum to boron tribromide, by focusing on the amount of red shift appearing with LA binding and ordering with LA electron-withdrawing capacity. An agreement with experiment is demonstrated in two respects: the difference between the transition energy of the adducts and the parent molecules before binding to LAs (Δ_{S1}) and the transition energy variation as a function of LA acidity. The difference between experimental and calculated Δ_{S1} is about 0.1 eV. The best agreement with experiment is observed for the J09G1 series using the APFD functional coupled with the dichlorobenzene solvent model.

Figure 3 summarizes the correlation between experimental and calculated values for optical transition energies. A correlation is statistically established across all methods used in this study (i.e., for both CAM-B3LYP-D3 and APFD models and for calculations in vacuum and solvent). Hence, these computational approaches are able to capture the effect of the relative strength of LAs on the optical transitions of the adducts. A linear fit with a slope close to 1 (0.94) and a small *y*-intercept (0.08) are observed for the APFD calculations with implicit *o*-dichlorobenzene. This indicates quantitative predictive capacity of this model for direct application to novel adducts. Yet, the strong R^2 for each of the four approaches shown in Figure 3 suggests that any method could be suitable for predictive simulations with use of a linear fit employing a trial set of experimental and computational data.

The observed agreement between theory and experiment allows us to propose a quantum descriptor of LAs quantifying their influence on optoelectronic properties of conjugated molecules upon formation of adducts. As illustrated in Figure 1 and detailed in the NBO analysis, the absorption red shift of D−A systems is mainly caused by lowering of LUMO of the acceptor due to charge redistribution from the nitrogen lone pair to the LA. Thus, following our approach developed by Zhugayevych et al.,[35] the change of the LUMO of a representative LB (model system) upon adduct formation with a LA defines the descriptor of that acid. For the considered PT/BT acceptors, the possible smallest model systems naturally include pyridine and 1,2,5-thiadiazole. Benchmarking of this descriptor for 13 LAs (Figures S3−S6) shows a linear correlation with the absorption red shifts (R^2 = 0.97).

For J11G3 and J11G8 adducts, the discrepancies between TD-DFT and experiments are larger. In these molecules, our calculations show that the binding to LAs causes a significant deformation of the backbone, decreasing its conjugation (Figure S1). These deformations reduce the calculated red shift in the adducts. In experimental data, the deformation might be compensated by other intermolecular interactions, for example, with the solvent environment,[26] that are not explicitly included in our current simulations. In the future work, we plan to investigate these effects.

An important question is how the red shift in optical spectra depends on the amount of charge transferred. Figure S7 shows that there is no overall *general* correlation between these two quantities. There is an apparent correlation for the aluminum-based LA family when the red shift increases with an increase of the charge transfer amount. In contrast, a slightly inverse dependence is observed for boron-based LAs in adducts with J09G1, when the red shift decreases with an increase of the charge transfer amount. Thus, although charge transfer provides a qualitative explanation of the observed red shifts in the adducts, a quantitative agreement with the observed trends across the series that can be captured with ab initio calculations cannot be uniformly mapped to this simplified single descriptor.

Finally, we analyze the hole and electron orbitals dominating the S_0−S_1 transition using the well-established natural transition orbitals (NTOs)[54] approach. Figure 4 depicts the electron and hole NTOs for isolated J09G1 as well as with its BCF adduct. Similar to the molecular orbital picture in Figure S2, the electron NTO also shows that LA binding enhances localization of the excited electron onto the acceptor region of the adduct compared to that of the parent molecule where the

DOI: 10.1021/acs.jpclett.9b01572
J. Phys. Chem. Lett. 2019, 10, 4632−4638

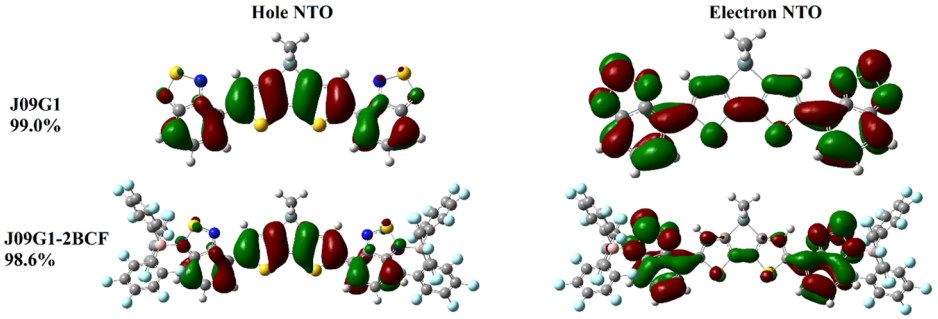

Figure 4. Hole and electron NTOs of J09G1 and J09−2BCF systems. The calculations were carried out with the APFD model and *o*-dichlorobenzene solvent medium. The percentage indicates participation of a given NTO pair in the multiconfigurational S_0−S_1 transition to the excited state.

electron delocalizes across the donor and acceptor moieties. The localization of the electron NTO on an acceptor unit upon binding with BCF is also evident in J11G3 and is less pronounced for J11G8 (Figure S8). In contrast, the hole NTO remains essentially unchanged upon the LA binding.

In summary, we demonstrate that, with appropriate choice of calculation methods, DFT can provide a powerful modeling tool to analyze elemental physical processes involving the formation of CM−LA adducts and predict their optical properties. Population analysis shows a noticeable amount of charge withdrawn from the acceptor moiety of the molecules by LAs, indicating a fractional electron transfer from CM to LA. This process was hypothesized to cause the experimental red shift in absorption spectra upon LA binding. This conjecture is confirmed with all of our TD-DFT simulations qualitatively predicting the red shift trends for the lowest optical transition for all molecular families studied. The APFD density functional coupled with implicit solvent models provides the best quantitative agreement with experimental absorption data and may be well-suited for simulating other CM−LA adducts and predictive applications. Finally, it is worth noting that while the red shifts are pronounced and are reproduced well in calculations, the underlying charge transfer is only partial and is relatively small. It seems that charge transfer alone does not explain experimentally observed carrier doping effects in polymers after LA additions. Exploring other contributing phenomena will be a subject of our future studies.

■ ASSOCIATED CONTENT

Supporting Information

The Supporting Information is available free of charge on the ACS Publications website at DOI: 10.1021/acs.jpclett.9b01572.

Model compounds, molecular properties of parent molecules and adducts, charge transfer quantification, LUMO plots, experimental and TDDFT-calculated S_1 transitions, molecular orbital diagrams, correlation plots, and hole and electron NTO (PDF)

■ AUTHOR INFORMATION

Corresponding Authors

*E-mail: serg@lanl.gov (S.T.).
*E-mail: emily.jarvis@lmu.edu (E.A.J.).

ORCID

Hung Phan: 0000-0001-5774-0390
Andriy Zhugayevych: 0000-0003-4713-1289
Guillermo C. Bazan: 0000-0002-2537-0310
Thuc-Quyen Nguyen: 0000-0002-8364-7517
Sergei Tretiak: 0000-0001-5547-3647

Notes

The authors declare no competing financial interest.

■ ACKNOWLEDGMENTS

This work is supported by the U.S. Department of Energy, Office of Science, Office of Basic Energy Sciences, under Award Number DE-SC0017659. H.P. acknowledge financial support of Fulbright University Vietnam in the form of a Professional Development Fund. This work was performed, in part, at the Center for Integrated Nanotechnologies (CINT), an Office of Science User Facility operated for the U.S. Department of Energy (DOE) Office of Science by Los Alamos National Laboratory and Sandia National Laboratories. We acknowledge support from the Center for Scientific Computing from the CNSI, MRL: an NSF MRSEC (DMR-1720256) and NSF CNS-1725797.

■ REFERENCES

(1) Salzmann, I.; Heimel, G.; Oehzelt, M.; Winkler, S.; Koch, N. Molecular Electrical Doping of Organic Semiconductors: Fundamental Mechanisms and Emerging Dopant Design Rules. *Acc. Chem. Res.* **2016**, *49* (3), 370−378.
(2) Rao, A.; Friend, R. H. Harnessing Singlet Exciton Fission to Break the Shockley-Queisser Limit. *Nat. Rev. Mater.* **2017**, *2* (11), 17063.
(3) Zhang, J.; Xu, W.; Sheng, P.; Zhao, G.; Zhu, D. Organic Donor-Acceptor Complexes as Novel Organic Semiconductors. *Acc. Chem. Res.* **2017**, *50* (7), 1654−1662.
(4) Benduhn, J.; Tvingstedt, K.; Piersimoni, F.; Ullbrich, S.; Fan, Y.; Tropiano, M.; McGarry, K. A.; Zeika, O.; Riede, M. K.; Douglas, C. J.; et al. Intrinsic Non-Radiative Voltage Losses in Fullerene-Based Organic Solar Cells. *Nat. Energy* **2017**, *2* (6), nenergy201753.
(5) Kilina, S.; Kilin, D.; Tretiak, S. Light-Driven and Phonon-Assisted Dynamics in Organic and Semiconductor Nanostructures. *Chem. Rev.* **2015**, *115* (12), 5929−5978.
(6) Janssen, R. A. J.; Nelson, J. Factors Limiting Device Efficiency in Organic Photovoltaics. *Adv. Mater.* **2013**, *25* (13), 1847−1858.
(7) Adachi, C. Third-Generation Organic Electroluminescence Materials. *Jpn. J. Appl. Phys.* **2014**, *53* (6), 060101.
(8) Sirringhaus, H. 25th Anniversary Article: Organic Field-Effect Transistors: The Path Beyond Amorphous Silicon. *Adv. Mater.* **2014**, *26* (9), 1319−1335.
(9) Collins, S. D.; Ran, N. A.; Heiber, M. C.; Nguyen, T.-Q. Small Is Powerful: Recent Progress in Solution-Processed Small Molecule Solar Cells. *Adv. Energy Mater.* **2017**, *7* (10), 1602242.

DOI: 10.1021/acs.jpclett.9b01572
J. Phys. Chem. Lett. 2019, 10, 4632−4638

(10) Noriega, R.; Rivnay, J.; Vandewal, K.; Koch, F. P. V.; Stingelin, N.; Smith, P.; Toney, M. F.; Salleo, A. A General Relationship between Disorder, Aggregation and Charge Transport in Conjugated Polymers. *Nat. Mater.* **2013**, *12* (11), 1038−1044.
(11) Rivnay, J.; Inal, S.; Salleo, A.; Owens, R. M.; Berggren, M.; Malliaras, G. G. Organic Electrochemical Transistors. *Nat. Rev. Mater.* **2018**, *3* (2), 17086.
(12) Welch, G. C.; Coffin, R.; Peet, J.; Bazan, G. C. Band Gap Control in Conjugated Oligomers via Lewis Acids. *J. Am. Chem. Soc.* **2009**, *131* (31), 10802−10803.
(13) Welch, G. C.; Bazan, G. C. Lewis Acid Adducts of Narrow Band Gap Conjugated Polymers. *J. Am. Chem. Soc.* **2011**, *133* (12), 4632−4644.
(14) Zalar, P.; Henson, Z. B.; Welch, G. C.; Bazan, G. C.; Nguyen, T.-Q. Color Tuning in Polymer Light-Emitting Diodes with Lewis Acids. *Angew. Chem.* **2012**, *124* (30), 7613−7616.
(15) Zalar, P.; Kuik, M.; Henson, Z. B.; Woellner, C.; Zhang, Y.; Sharenko, A.; Bazan, G. C.; Nguyen, T.-Q. Increased Mobility Induced by Addition of a Lewis Acid to a Lewis Basic Conjugated Polymer. *Adv. Mater.* **2014**, *26* (5), 724−727.
(16) Han, Y.; Barnes, G.; Lin, Y.-H.; Martin, J.; Al-Hashimi, M.; AlQaradawi, S. Y.; Anthopoulos, T. D.; Heeney, M. Doping of Large Ionization Potential Indenopyrazine Polymers via Lewis Acid Complexation with Tris(Pentafluorophenyl)Borane: A Simple Method for Improving the Performance of Organic Thin-Film Transistors. *Chem. Mater.* **2016**, *28* (21), 8016−8024.
(17) Randell, N. M.; Fransishyn, K. M.; Kelly, T. L. Lewis Acid−Base Chemistry of 7-Azaisoindigo-Based Organic Semiconductors. *ACS Appl. Mater. Interfaces* **2017**, *9* (29), 24788−24796.
(18) Panidi, J.; Paterson, A. F.; Khim, D.; Fei, Z.; Han, Y.; Tsetseris, L.; Vourlias, G.; Patsalas, P. A.; Heeney, M.; Anthopoulos, T. D. Remarkable Enhancement of the Hole Mobility in Several Organic Small-Molecules, Polymers, and Small-Molecule:Polymer Blend Transistors by Simple Admixing of the Lewis Acid p-Dopant B(C6F5)3. *Adv. Sci.* **2018**, *5* (1), 1700290.
(19) Huang, J.; Li, Y.; Wang, Y.; Meng, H.; Yan, D.; Jiang, B.; Wei, Z.; Zhan, C. A Lewis Acid-Base Chemistry Approach towards Narrow Bandgap Dye Molecules. *Dyes Pigm.* **2018**, *153*, 1−9.
(20) Yan, H.; Chen, J.; Zhou, K.; Tang, Y.; Meng, X.; Xu, X.; Ma, W. Lewis Acid Doping Induced Synergistic Effects on Electronic and Morphological Structure for Donor and Acceptor in Polymer Solar Cells. *Adv. Energy Mater.* **2018**, *8* (19), 1703672.
(21) Li, Y.; Meng, H.; Li, Y.; Pang, B.; Luo, G.; Huang, J. Adjusting the Energy Levels and Bandgaps of Conjugated Polymers via Lewis Acid−Base Reactions. *New J. Chem.* **2018**, *42* (23), 18961−18968.
(22) Yurash, B.; Leifert, D.; Reddy, G. N. M.; Cao, D. X.; Biberger, S.; Brus, V. V.; Seifrid, M.; Santiago, P. J.; Köhler, A.; Chmelka, B. F.; et al. Atomic-Level Insight into the Postsynthesis Band Gap Engineering of a Lewis Base Polymer Using Lewis Acid Tris-(Pentafluorophenyl)Borane. *Chem. Mater.* **2019**, DOI: 10.1021/acs.chemmater.9b01224.
(23) Min, Y.; Dou, C.; Tian, H.; Geng, Y.; Liu, J.; Wang, L. N-Type Azaacenes Containing B←N Units. *Angew. Chem.* **2018**, *130* (7), 2018−2022.
(24) Grandl, M.; Sun, Y.; Pammer, F. Electronic and Structural Properties of N → B-Ladder Boranes with High Electron Affinity. *Org. Chem. Front.* **2018**, *5* (3), 336−352.
(25) Hayashi, S.; Asano, A.; Koizumi, T. Modification of Pyridine-Based Conjugated Polymer Films via Lewis Acid: Halochromism, Characterization and Macroscopic Gradation Patterning. *Polym. Chem.* **2011**, *2* (12), 2764−2766.
(26) Hansmann, M. M.; López-Andarias, A.; Rettenmeier, E.; Egler-Lucas, C.; Rominger, F.; Hashmi, A. S. K.; Romero-Nieto, C. $B(C_6F_5)_3$: A Lewis Acid That Brings the Light to the Solid State. *Angew. Chem., Int. Ed.* **2016**, *55* (3), 1196−1199.
(27) Poverenov, E.; Zamoshchik, N.; Patra, A.; Ridelman, Y.; Bendikov, M. Unusual Doping of Donor−Acceptor-Type Conjugated Polymers Using Lewis Acids. *J. Am. Chem. Soc.* **2014**, *136* (13), 5138−5149.
(28) Pingel, P.; Arvind, M.; Kölln, L.; Steyrleuthner, R.; Kraffert, F.; Behrends, J.; Janietz, S.; Neher, D. P-Type Doping of Poly(3-Hexylthiophene) with the Strong Lewis Acid Tris-(Pentafluorophenyl)Borane. *Adv. Electron. Mater.* **2016**, *2* (10), 1600204.
(29) Wang, W.; Chen, C.; Tollan, C.; Yang, F.; Qin, Y.; Knez, M. Efficient and Controllable Vapor to Solid Doping of the Polythiophene P3HT by Low Temperature Vapor Phase Infiltration. *J. Mater. Chem. C* **2017**, *5* (10), 2686−2694.
(30) Mebs, S.; Grabowsky, S.; Förster, D.; Kickbusch, R.; Hartl, M.; Daemen, L. L.; Morgenroth, W.; Luger, P.; Paulus, B.; Lentz, D. Charge Transfer via the Dative N−B Bond and Dihydrogen Contacts. Experimental and Theoretical Electron Density Studies of Small Lewis Acid−Base Adducts. *J. Phys. Chem. A* **2010**, *114* (37), 10185−10196.
(31) Brandenburg, J. G.; Grimme, S. Organic Crystal Polymorphism: A Benchmark for Dispersion-Corrected Mean-Field Electronic Structure Methods. *Acta Crystallogr., Sect. B: Struct. Sci., Cryst. Eng. Mater.* **2016**, *72* (4), 502−513.
(32) Zhugayevych, A.; Mazaleva, O.; Naumov, A.; Tretiak, S. Lowest-Energy Crystalline Polymorphs of P3HT. *J. Phys. Chem. C* **2018**, *122* (16), 9141−9151.
(33) van der Poll, T. S.; Zhugayevych, A.; Chertkov, E.; Bakus, R. C.; Coughlin, J. E.; Teat, S. J.; Bazan, G. C.; Tretiak, S. Polymorphism of Crystalline Molecular Donors for Solution-Processed Organic Photovoltaics. *J. Phys. Chem. Lett.* **2014**, *5* (15), 2700−2704.
(34) Coughlin, J. E.; Zhugayevych, A.; Bakus, R. C.; van der Poll, T. S.; Welch, G. C.; Teat, S. J.; Bazan, G. C.; Tretiak, S. A Combined Experimental and Theoretical Study of Conformational Preferences of Molecular Semiconductors. *J. Phys. Chem. C* **2014**, *118* (29), 15610−15623.
(35) Zhugayevych, A.; Postupna, O.; Wang, H.-L.; Tretiak, S. Modification of Optoelectronic Properties of Conjugated Oligomers Due to Donor/Acceptor Functionalization: DFT Study. *Chem. Phys.* **2016**, *481*, 133−143.
(36) Zhang, C.-R.; Sears, J. S.; Yang, B.; Aziz, S. G.; Coropceanu, V.; Brédas, J.-L. Theoretical Study of the Local and Charge-Transfer Excitations in Model Complexes of Pentacene-C60 Using Tuned Range-Separated Hybrid Functionals. *J. Chem. Theory Comput.* **2014**, *10* (6), 2379−2388.
(37) Sutton, C.; Sears, J. S.; Coropceanu, V.; Brédas, J.-L. Understanding the Density Functional Dependence of DFT-Calculated Electronic Couplings in Organic Semiconductors. *J. Phys. Chem. Lett.* **2013**, *4* (6), 919−924.
(38) Guido, C. A.; Jacquemin, D.; Adamo, C.; Mennucci, B. Electronic Excitations in Solution: The Interplay between State Specific Approaches and a Time-Dependent Density Functional Theory Description. *J. Chem. Theory Comput.* **2015**, *11* (12), 5782−5790.
(39) Tsuneda, T.; Singh, R. K.; Nakata, A. Relationship between Orbital Energy Gaps and Excitation Energies for Long-chain Systems. *J. Comput. Chem.* **2016**, *37* (16), 1451−1462.
(40) Sun, H.; Autschbach, J. Electronic Energy Gaps for π-Conjugated Oligomers and Polymers Calculated with Density Functional Theory. *J. Chem. Theory Comput.* **2014**, *10* (3), 1035−1047.
(41) Tomasi, J.; Mennucci, B.; Cammi, R. Quantum Mechanical Continuum Solvation Models. *Chem. Rev.* **2005**, *105* (8), 2999−3094.
(42) Cossi, M.; Rega, N.; Scalmani, G.; Barone, V. Energies, Structures, and Electronic Properties of Molecules in Solution with the C-PCM Solvation Model. *J. Comput. Chem.* **2003**, *24* (6), 669−681.
(43) Takano, Y.; Houk, K. N. Benchmarking the Conductor-like Polarizable Continuum Model (CPCM) for Aqueous Solvation Free Energies of Neutral and Ionic Organic Molecules. *J. Chem. Theory Comput.* **2005**, *1* (1), 70−77.
(44) Jonas, V.; Frenking, G.; Reetz, M. T. Comparative Theoretical Study of Lewis Acid-Base Complexes of BH3, BF3, BCl3, AlCl3, and SO2. *J. Am. Chem. Soc.* **1994**, *116* (19), 8741−8753.

DOI: 10.1021/acs.jpclett.9b01572
J. Phys. Chem. Lett. 2019, 10, 4632−4638

(45) Mo, Y.; Gao, J. Polarization and Charge-Transfer Effects in Lewis Acid−Base Complexes. *J. Phys. Chem. A* **2001**, *105* (26), 6530−6536.
(46) Yanai, T.; Tew, D. P.; Handy, N. C. A New Hybrid Exchange−Correlation Functional Using the Coulomb-Attenuating Method (CAM-B3LYP). *Chem. Phys. Lett.* **2004**, *393* (1), 51−57.
(47) Grimme, S.; Ehrlich, S.; Goerigk, L. Effect of the Damping Function in Dispersion Corrected Density Functional Theory. *J. Comput. Chem.* **2011**, *32* (7), 1456−1465.
(48) Austin, A.; Petersson, G. A.; Frisch, M. J.; Dobek, F. J.; Scalmani, G.; Throssell, K. A Density Functional with Spherical Atom Dispersion Terms. *J. Chem. Theory Comput.* **2012**, *8* (12), 4989−5007.
(49) Foster, J. P.; Weinhold, F. Natural Hybrid Orbitals. *J. Am. Chem. Soc.* **1980**, *102* (24), 7211−7218.
(50) Reed, A. E.; Weinstock, R. B.; Weinhold, F. Natural Population Analysis. *J. Chem. Phys.* **1985**, *83* (2), 735−746.
(51) Hirshfeld, F. L. Bonded-Atom Fragments for Describing Molecular Charge Densities. *Theor. Chim. Acta* **1977**, *44* (2), 129−138.
(52) Marenich, A. V.; Jerome, S. V.; Cramer, C. J.; Truhlar, D. G. Charge Model 5: An Extension of Hirshfeld Population Analysis for the Accurate Description of Molecular Interactions in Gaseous and Condensed Phases. *J. Chem. Theory Comput.* **2012**, *8* (2), 527−541.
(53) Bredas, J.-L. Mind the Gap! *Mater. Horiz.* **2014**, *1* (1), 17−19.
(54) Martin, R. L. Natural Transition Orbitals. *J. Chem. Phys.* **2003**, *118* (11), 4775−4777.

DOI: 10.1021/acs.jpclett.9b01572
J. Phys. Chem. Lett. 2019, 10, 4632−4638

Supporting Information

Tuning Optical Properties of Conjugated Molecules by Lewis Acids: Insights from Electronic Structure Modeling

Hung Phan,[1,2] Thomas J. Kelly,[3] Andriy Zhugayevych,[4] Guillermo C. Bazan,[2] Thuc-Quyen Nguyen,[2] Emily Jarvis,[3*] Sergei Tretiak[4,5*]

[1]Fulbright University Vietnam, Ho Chi Minh city, Vietnam

[2]Center for Polymer and Organic Solids (CPOS), University of California Santa Barbara, Santa Barbara, California, USA

[3]Department of Chemistry & Biochemistry, Loyola Marymount University, Los Angeles, California, USA

[4]Skolkovo Institute of Science and Technology, Moscow 143026, Russia

[5]Theoretical Division and Center for Integrated Nanotechnologies, Los Alamos National Laboratory, Los Alamos, New Mexico, USA

Section S1. Model compounds (Figure 1)

J09G1 is the first molecule that Welch and coworkers[1] showed to bind with a series of LAs that varied in acidity. The resulting adducts display pronounced red-shift in optical absorption, which increases with the strength of the LA. J09G1-2BCF was also isolated and studied by ^{1}H, ^{11}B and ^{19}F NMR spectroscopies. This work concluded that the two BCF are bound to the two BT units at the opposite ends of J09G1.[1] In addition, a single crystal structure of the BCF adduct with only the acceptor molecule (BT-Br),[1] verified that BCF binds to nitrogen. The reduced bandgaps of the adducts were also confirmed in DFT calculations at the B3LYP/6-31G level. J11G3 was synthesized in a subsequent study.[2] There, it was demonstrated that LA can also bind to the more sterically hindered N atom of the BT acceptor sandwiched between two donor moieties (Figure 1). J11G8, which changes BT to PT was also studied on the basis that pyridine is known to bind BCF,[2–4] and pyridyl N-atom is hypothesized to have higher basicity than the azole N-atom of BT.[2]

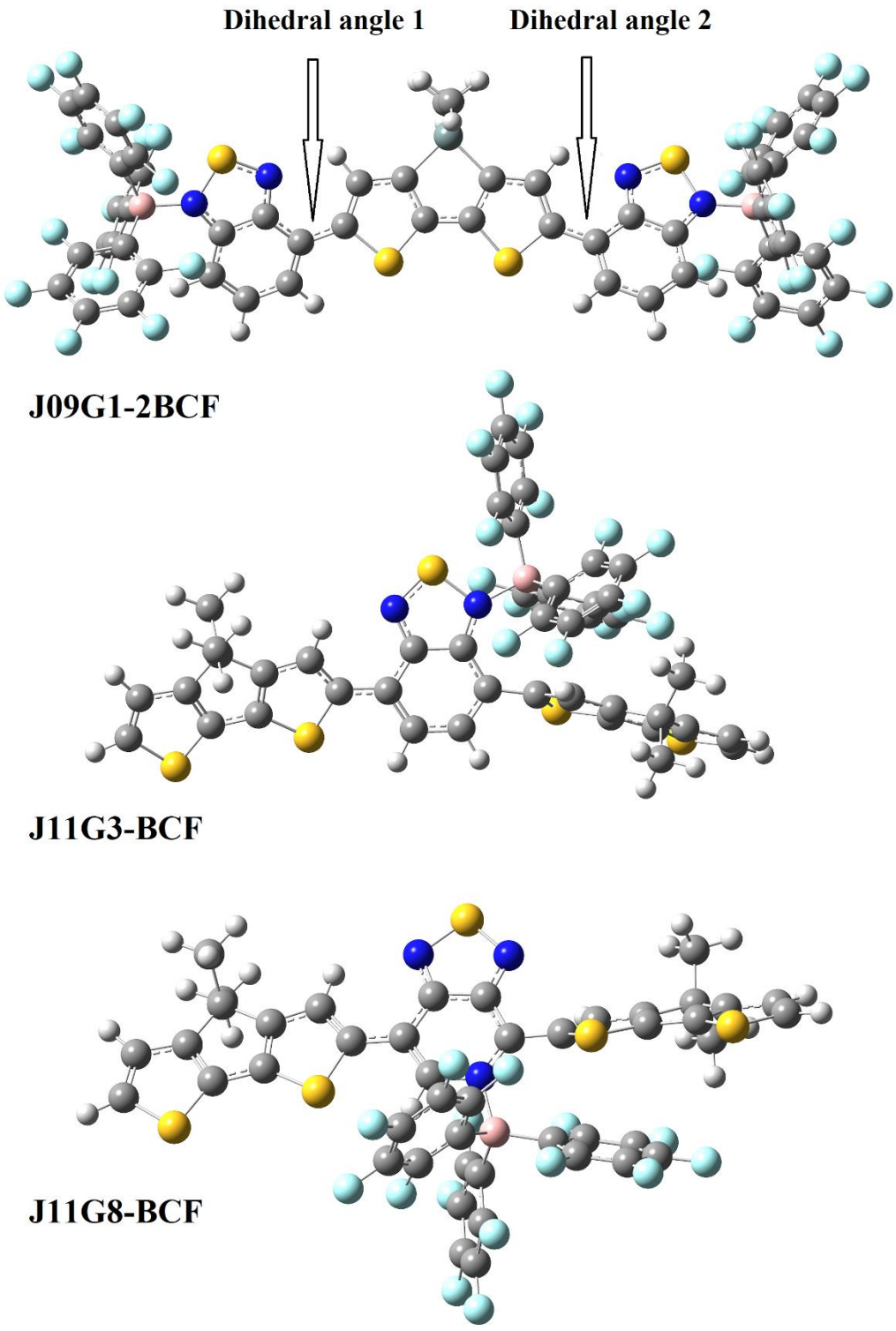

Figure S1. Optimized structures of three adducts J09G1-2BCF, J11G3-BCF and J11G8-BCF. The dihedral angle on the left and right is defined as dihedral angle 1 and 2, respectively in Table S1.

Table S1. Molecular properties of optimized parent molecules and adducts. The stabilization energy is calculated by subtracting the total energy of the parent conjugated molecule and the Lewis acid from total energy of the adduct. For adducts with two Lewis acids binding, the stabilization energy is divided by two to get the average stabilization energy for one LA-LB bond.

Adducts	LA-LB bond length	Stabilization Energy for one LA-LB bond (kJ/mol)	Change in Dihedral angle 1	Change in Dihedral angle 2
J09G1-2AlMe$_3$	2.07	-101.2	0.5	0.6
J09G1-2AlEtCl$_2$	1.99	-150.3	7.8	7.9
J09G1-2BCF	1.62	-120.3	8.7	8.5
J09G1-2BCl$_3$	1.58	-116.4	8.9	9.0
J09G1-2BBr$_3$	1.56	-140.3	8.8	8.9
J11G3-BCF	1.64	-104.6	9.2	67.6
J11G8-BCF	1.66	-108.7	11.1	58.0

Table S2. Charge transfer quantification of CM-LA adducts including J09G1, J11G3 and J11G8. The values were calculated with APFD and CM5 population method in vacuum. Compared to NBO, CM5 predicts a higher amount of charge transfer for all adducts, and a smaller distinction between aluminum-based LAs (~0.30 – 0.35e) and boron-based LAs (~0.4 – 0.43e).

Molecules & Adducts	CM5 - Vacuum			
	Σ_{LB}	Δ_{LB}	Δ_{LA}	$\Delta_{LB} + \Delta_{LA}$
J09G1	-0.027			
J09G1-AlMe$_3$	0.247	0.273	-0.302	-0.028
J09G1-AlEtCl$_2$	0.255	0.282	-0.327	-0.045
J09G1-AlCF	0.271	0.298	-0.349	-0.051
J09G1-BCF	0.353	0.379	-0.431	-0.051
J09G1-BCl$_3$	0.343	0.370	-0.421	-0.051
J09G1-BBr$_3$	0.321	0.347	-0.397	-0.050
J11G3	-0.063			
J11G3-BCF	0.278	0.341	-0.420	-0.078
J11G8	-0.114			
J11G8-BCF	0.168	0.282	-0.459	-0.177

Σ_{LB}: *The total net charge of all atoms in LB fragment of the molecule*
Δ_{LB}: *The change in total net charge of LB fragment before and after binding to LA*
Δ_{LA}: *The change in total net charge of LA fragment before and after binding to LA*

Table S3. Charge transfer quantification of CM-LA adducts of J09G1, J11G3 and J11G8 in ground states. The values were calculated with CAM-B3LYP/6-311G(d,p) level of theory with GD3BJ dispersion function.

Molecules & Adducts	NBO - Vacuum				NBO - Dichlorobenzene				CM5 - Vacuum			
	Σ_{LB}	Δ_{LB}	Δ_{LA}	$\Delta_{LB} + \Delta_{LA}$	Σ_{LB}	Δ_{LB}	Δ_{LA}	$\Delta_{LB} + \Delta_{LA}$	Σ_{LB}	Δ_{LB}	Δ_{LA}	$\Delta_{LB} + \Delta_{LA}$
J09G1	-0.059				-0.049				-0.016			
J09G1-$AlMe_3$	0.062	-0.137	0.121	-0.016	0.083	-0.152	0.133	-0.020	0.272	-0.313	0.288	-0.025
J09G1-$AlEtCl_2$	0.056	-0.140	0.115	-0.025	0.082	-0.163	0.131	-0.032	0.280	-0.335	0.296	-0.039
J09G1-BCF	0.289	-0.377	0.347	-0.029	0.312	-0.395	0.361	-0.034	0.377	-0.437	0.393	-0.045
J09G1-BCl_3	0.221	-0.308	0.279	-0.029	0.259	-0.349	0.308	-0.041	0.370	-0.430	0.386	-0.044
J09G1-BBr_3	0.196	-0.283	0.255	-0.028	0.235	-0.325	0.285	-0.041	0.352	-0.411	0.368	-0.043
J11G3	-0.128				-0.115				-0.037			
J11G3-BCF	0.220	-0.373	0.347	-0.025	0.249	-0.388	0.365	-0.024	0.319	-0.428	0.356	-0.072
J11G8	-0.169				-0.163				-0.079			
J11G8-BCF	0.111	-0.359	0.279	-0.079	0.150	-0.373	0.313	-0.060	0.226	-0.455	0.305	-0.149

Σ_{LB}: *The total net charge of all atoms in LB fragment of the molecule*
Δ_{LB}: *The change in total net charge of LB fragment before and after binding to LA*
Δ_{LA}: *The change in total net charge of LA fragment before and after binding to LA*

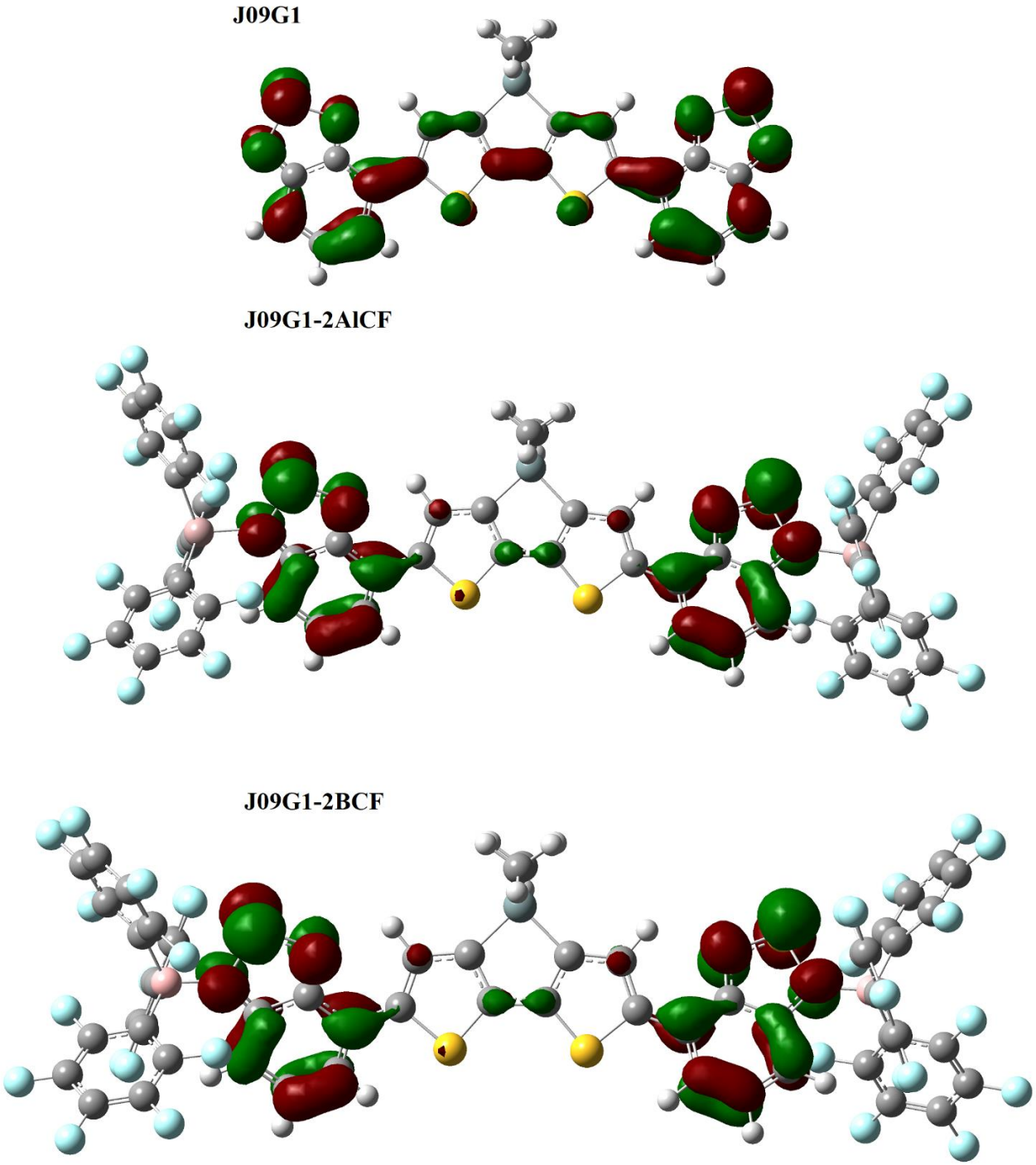

Figure S2. LUMO plots for J09G1, J09G1-2AlCF, and J09G1-2BCF systems showing the evolution of initially delocalized orbital in the parent molecule to a localized state in the acceptor region with LA binding.

Table S4. Experimental and TDDFT-calculated S_1 transition (eV) of CM-LA adducts.

Compounds	Experiments		CAM-B3LYP with GD3BJ				APFD			
	S1 (o-DCB)	Δ_{S1}	S1 (Vacuum)	$\Delta_{S1\text{-}Vac}$	S1 (o-DCB)	$\Delta_{S1\text{-}DCB}$	S1 (Vacuum)	$\Delta_{S1\text{-}Vac}$	S1 (o-DCB)	$\Delta_{S1\text{-}DCB}$
J09G1	**2.46**		**2.81**		**2.79**		**2.26**		**2.22**	
J09G1-2AlMe$_3$	2.16	0.30	2.61	0.19	2.60	0.18	2.00	0.26	1.94	0.29
J09G1-2AlEtCl$_2$	1.98	0.48	2.48	0.33	2.44	0.35	1.87	0.39	1.77	0.45
J09G1-2BCF	1.92	0.55	2.43	0.37	2.40	0.38	1.82	0.44	1.75	0.48
J09G1-2BCl$_3$	1.88	0.59	2.40	0.41	2.28	0.50	1.79	0.47	1.64	0.58
J09G1-2Br$_3$	1.82	0.64	2.37	0.43	2.26	0.52	1.76	0.50	1.62	0.60
J11G3	**2.18**		**2.47**		**2.46**		**1.93**		**1.88**	
J11G3-BCF	1.53	0.65	2.33	0.14	2.35	0.10	1.43	0.51	1.59	0.29
J11G8	**2.01**		**2.35**		**2.30**		**1.80**		**1.75**	
J11G8-BCF	1.65	0.36	2.27	0.08	2.37	-0.06	1.67	0.13	1.68	0.07

Δ_{S1}: *the difference between S1 energy of the adducts and the parent molecules.*

In term of comparing absolute values of experimental S_1 to calculated ones, the ones calculated from CAM-B3LYP-D3 are blue-shifted around 0.1-0.3 eV and the ones calculated from APFD red-shifted around 0.1-0.2 eV. This behavior is certainly related to the different Hartree-Fock exchange included in the two methods. CAM-B3LYP functional comprises of 0.19 Hartree–Fock (HF) plus 0.81 Becke 1988 (B88) exchange interaction at short-range, and 0.65 HF plus 0.35 B88 at long-range,[5] while APF has 0.23 HF exchange from the combination of B3PW91 and PBE1PBE hybrid functionals.[6]

S2. Quantum descriptors for the absorption redshift (Figure S3-S6)

The ΔE_{LUMO} (**Figure S4**) is the difference between the LUMO energy of the Lewis base and its value in the adduct with a given Lewis acid (**Figure S3**). The ΔE_{LUMO} and absorption redshift in a search for quantum descriptors was calculated with CAM-B3LYP/6-31G(d,p) method.

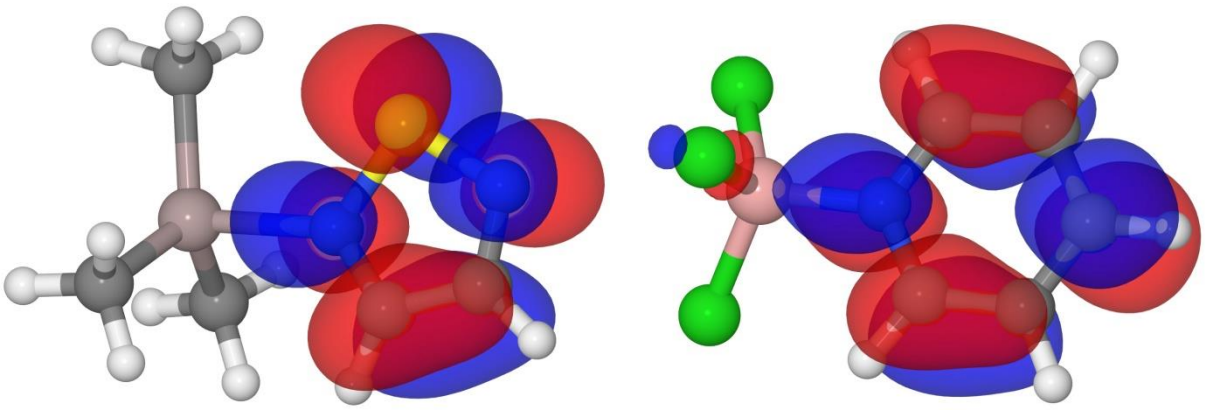

Figure S3. Example of two model adducts used for calculating quantum descriptors, $AlMe_3$ + 1,2,5-thiadiazole and BCl_3 + pyridine. The LUMO is shown.

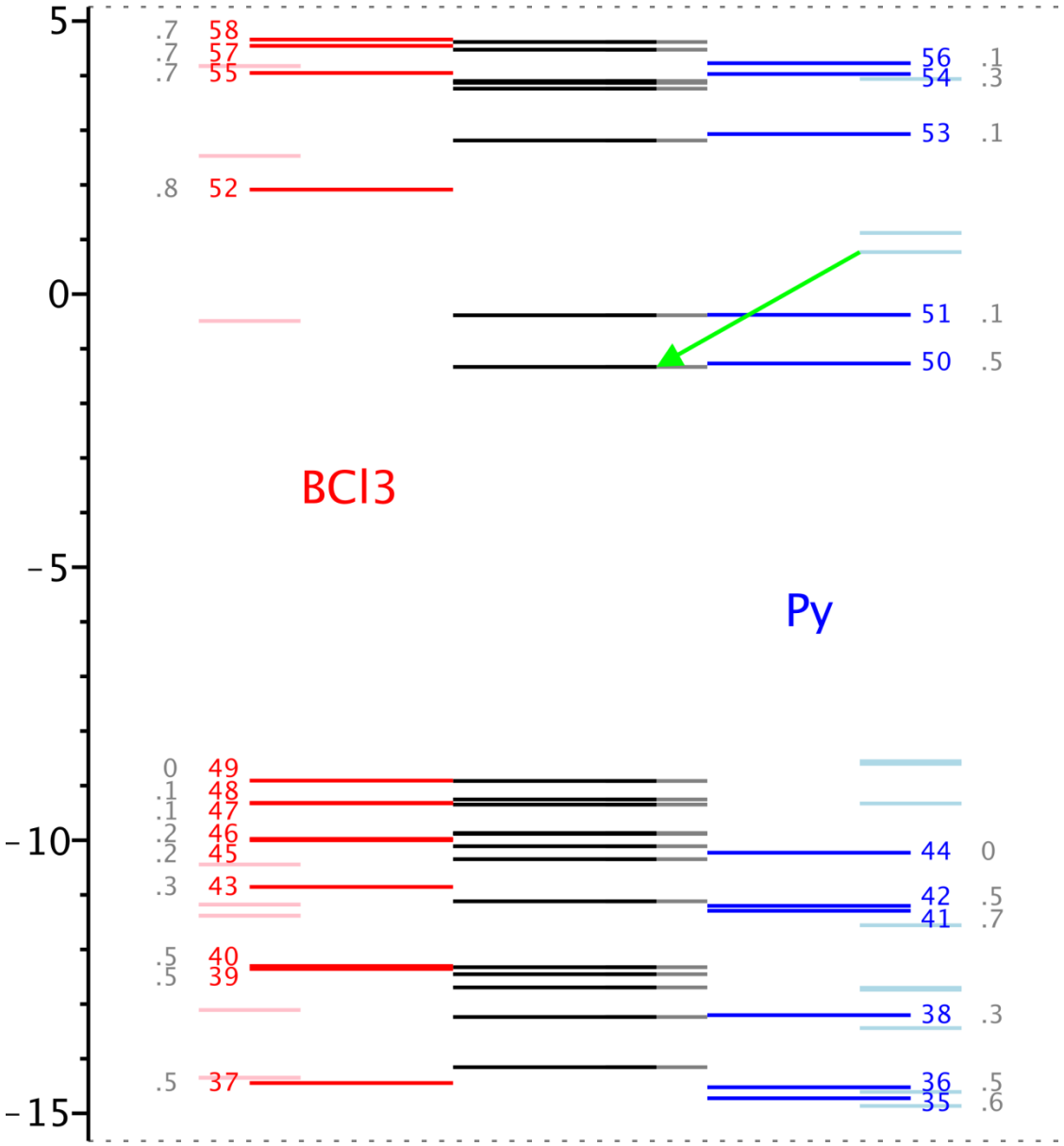

Figure S4. Molecular orbital (MO) diagram of the BCl_3 + pyridine adduct. The black colored set of MOs at the center are the eigenvalues of the Fock matrix of the entire adduct. The red and blue sets correspond to the eigenvalues of the orthogonal projections of the Fock matrix onto each of the two fragments (BCl_3 and pyridine) obtained using NBO basis. Together they form a complete basis and are numbered according to their energy. The gray colored numbers are the values of MO wave-function on the bridging atom. The light red and light blue sets correspond to the isolated fragments. The green arrow shows the change of LUMO of the Lewis base upon adduct formation, which the ΔE_{LUMO} descriptor proposed in this work.

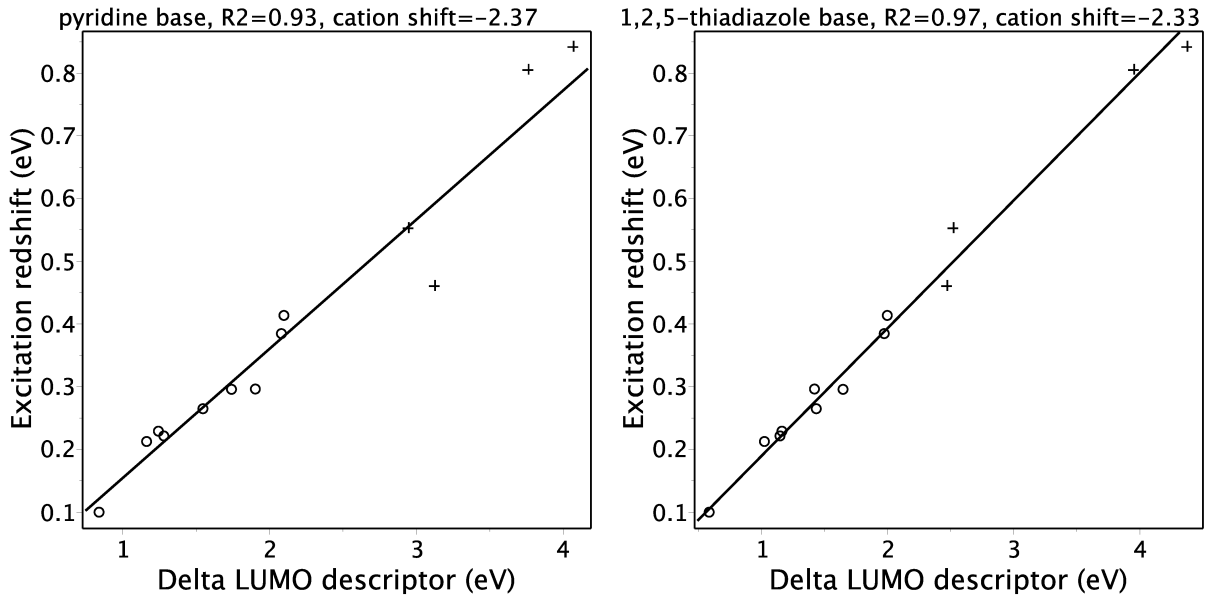

Figure S5. Correlation plots between the ΔE_{LUMO} descriptor of 13 Lewis acid (ClF, BMe_3, $AlMe_3$, BH_3, SO_3, BF_3, AlF_3, $AlCl_3$, BCl_3, Na^+, Li^+, Me^+, H^+) with the two different small Lewis bases and the absorption redshifts of these acids with J09G1. The least squares fitting is performed for the neutral bases, then the ΔE_{LUMO} values of all cations are shifted by the same value to match the linear fit.

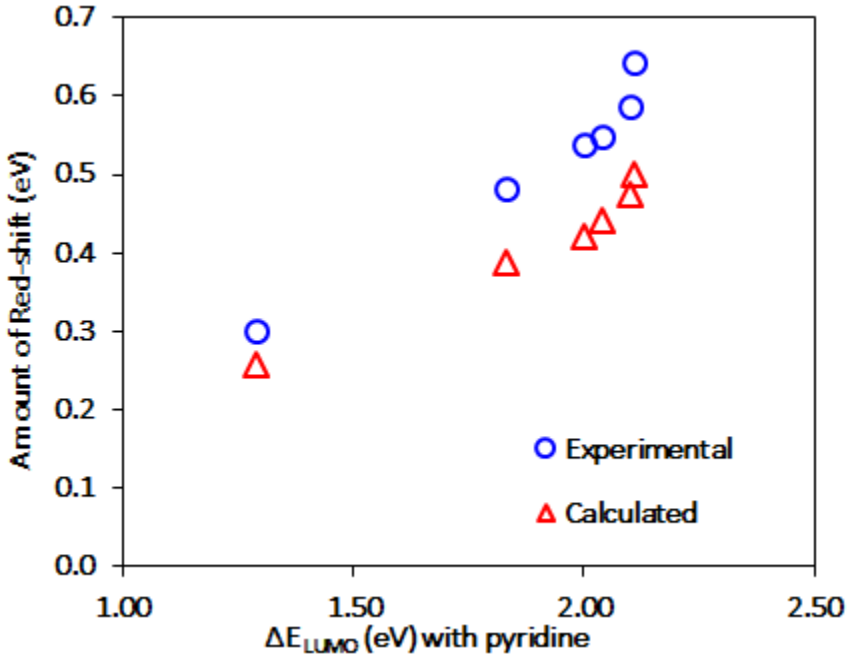

Figure S6. Correlation plots between the ΔE_{LUMO} descriptor of Lewis acid used in this study (**Table S4**) and the absorption redshift of those acids with J09G1, both calculated (APFD/6-311G(d,p)) and experimental.

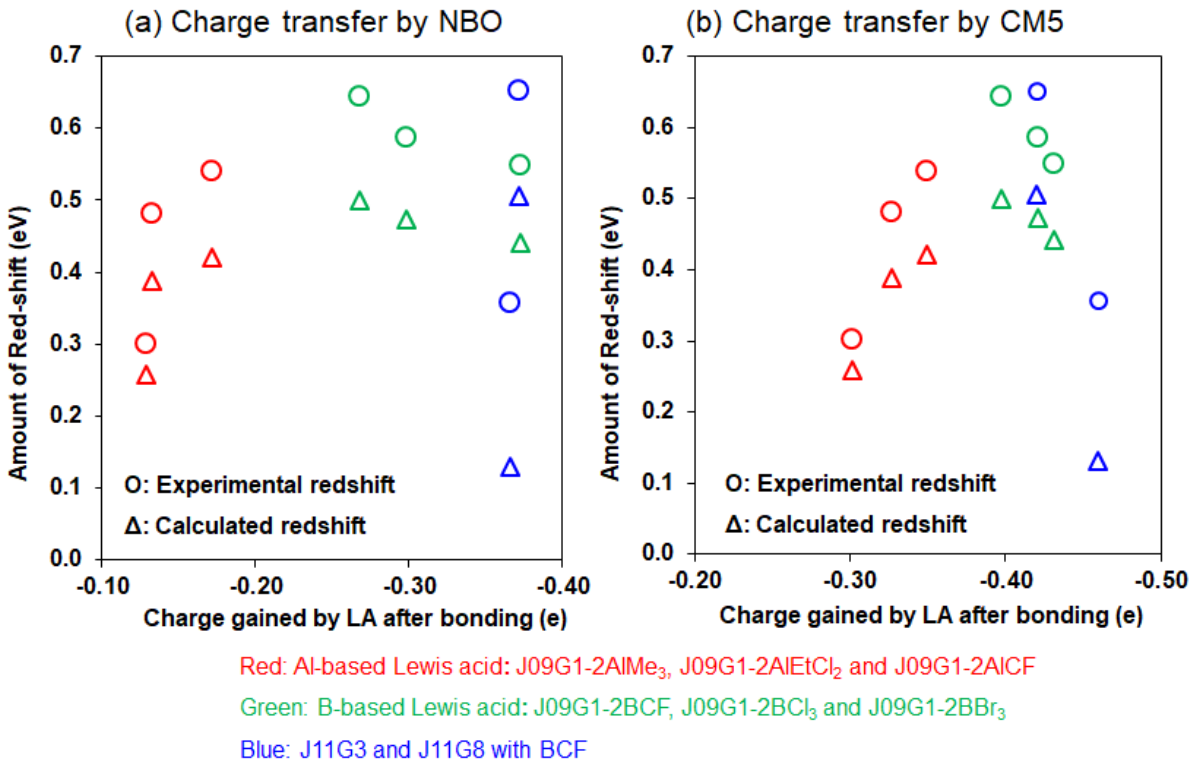

Figure S7. The relationship between the charge transfer amount partitioned by (a) NBO and (b) CM5 schemes, and the values of experimental (open circles) and calculated (open triangle) redshifts. All calculations here were carried out by the AFPD model in vacuum. Calculations performed with CAM-B3LYP-D3 and in DCB solvent, show similar results. In this case, we use the amount of charge gain by Lewis acid upon forming the adducts as the measure of charge transfer.

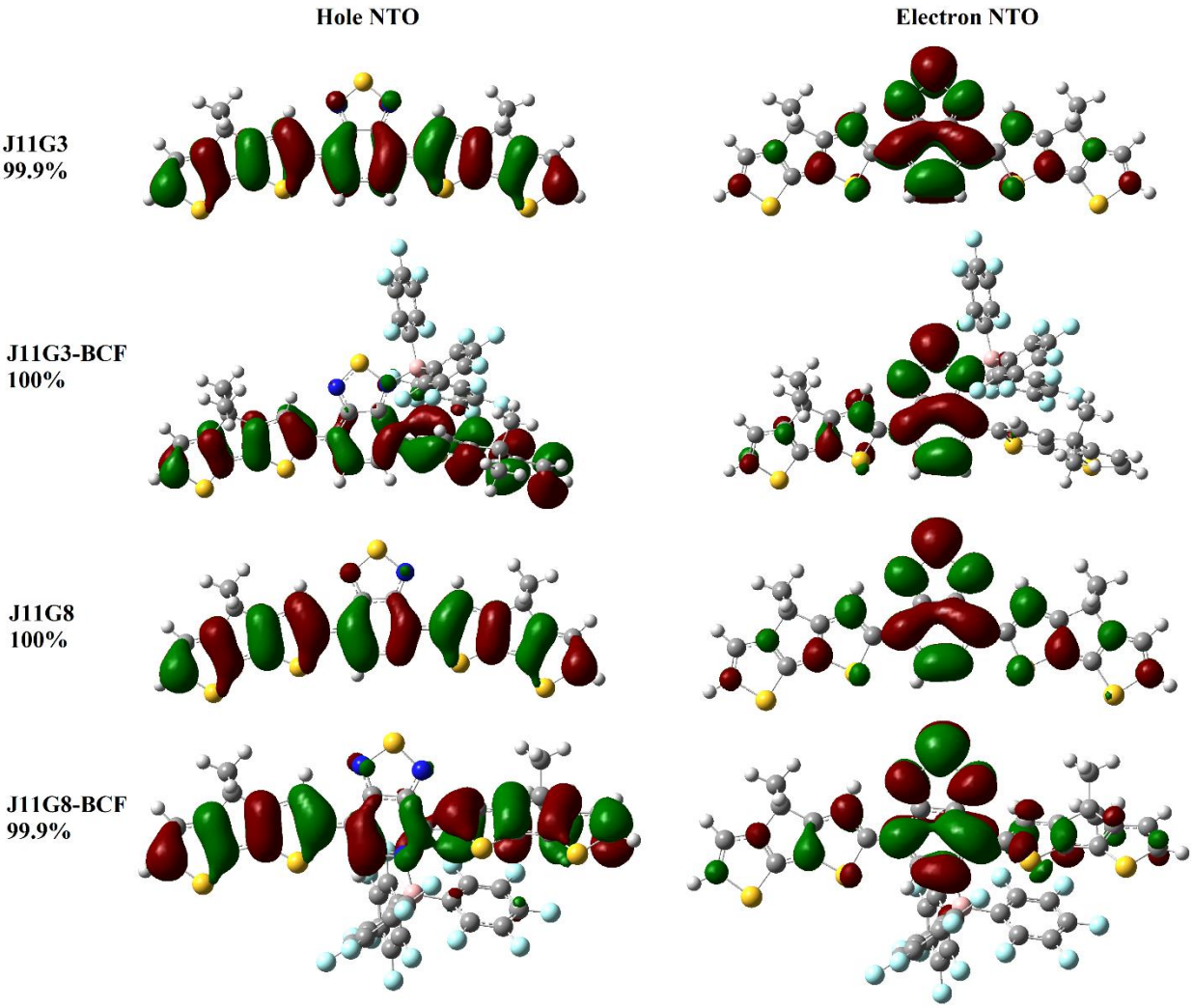

Figure S8. Hole and electron NTO of J11G3, J11G8 and their adducts, calculated with APFD functionals and o-DCB solvent medium.

References

(1) Welch, G. C.; Coffin, R.; Peet, J.; Bazan, G. C. Band Gap Control in Conjugated Oligomers via Lewis Acids. *J. Am. Chem. Soc.* **2009**, *131* (31), 10802–10803. https://doi.org/10.1021/ja902789w.

(2) Welch, G. C.; Bazan, G. C. Lewis Acid Adducts of Narrow Band Gap Conjugated Polymers. *J. Am. Chem. Soc.* **2011**, *133* (12), 4632–4644. https://doi.org/10.1021/ja110968m.

(3) Lesley, M. J. G.; Woodward, A.; Taylor, N. J.; Marder, T. B.; Cazenobe, I.; Ledoux, I.; Zyss, J.; Thornton, A.; Bruce, D. W.; Kakkar, A. K. Lewis Acidic Borane Adducts of Pyridines and Stilbazoles for Nonlinear Optics. *Chem. Mater.* **1998**, *10* (5), 1355–1365. https://doi.org/10.1021/cm9707519.

(4) Massey, A. G.; Park, A. J. Perfluorophenyl Derivatives of the Elements: VII. Further Studies on Tris(Pentafluorophenyl)Boron. *J. Organomet. Chem.* **1966**, *5* (3), 218–225. https://doi.org/10.1016/S0022-328X(00)80358-7.

(5) Yanai, T.; Tew, D. P.; Handy, N. C. A New Hybrid Exchange–Correlation Functional Using the Coulomb-Attenuating Method (CAM-B3LYP). *Chem. Phys. Lett.* **2004**, *393* (1), 51–57. https://doi.org/10.1016/j.cplett.2004.06.011.

(6) Austin, A.; Petersson, G. A.; Frisch, M. J.; Dobek, F. J.; Scalmani, G.; Throssell, K. A Density Functional with Spherical Atom Dispersion Terms. *J. Chem. Theory Comput.* **2012**, *8* (12), 4989–5007. https://doi.org/10.1021/ct300778e.